2013 NDIA GROUND VEHICLE SYSTEMS ENGINEERING AND TECHNOLOGY SYMPOSIUM
MODELING & SIMULATION, TESTING AND VALIDATION (MSTV) MINI-SYMPOSIUM
AUGUST 21-22, 2013 – TROY, MICHIGAN

TRACKED VEHICLE – SOFT SOIL INTERACTIONS AND DESIGN SENSITIVITIES FOR PATH CLEARING SYSTEMS UTILIZING MULTI-BODY DYNAMICS SIMULATION METHODS

Joseph B Raymond
Paramsothy Jayakumar, PhD
Vehicle Dynamics & Structures Modeling & Simulation
US Army TARDEC – Systems Integration & Engineering – Analytics
Warren, MI

ABSTRACT

Two notional path-clearing tracked-vehicle models are part of this exploration in assessing the capabilities and limitations of the state-of-the-art in tracked vehicle dynamics modeling and simulation over soft-soil terrain. Each vehicle utilized different path-clearing methods that presented challenges in modeling their interactions with the soil: one vehicle used a roller and rake combination. The roller pressured the soft soil while the rake sheared it. The other vehicle used a quickly rotating flail system that cleared a definitive path by impacting and flinging the soil away. One vehicle had a band track and the other had a segmented track introducing additional modeling challenges. Each of these design choices was independently varied and analyzed. Path clearing performances and design sensitivities to track properties were studied in addition to the effect of contact forces between track, road wheels, idler, and sprocket. Vehicle performance on differing soil types is also compared by means of load and acceleration time histories derived from complex multi-body dynamics simulations. Unique modeling methods to stretch the capability of the current state-of-the-art were paramount in enabling this study, and are discussed in detail.

INTRODUCTION

This study focuses on isolating and changing several important design variables while keeping most other parameters constant to maintain scientific integrity. Of note, the notional chassis was constant. The chassis was designed with the abstract goal of going most places that people can go. The chassis was thin enough to fit in most doorways, capable of going up most sloped terrain, and able to traverse cross country. The chassis had a set power output limit, which may be distributed as necessary between the prime-mover powertrain and the path-clearing implement. The sprocket, idler, and road wheel geometries were also held constant. The path-clearing implement, number of road wheels, track type and properties, and soil type were varied. Figure 1 and Figure 2 highlight these differences. A Design of Experiments (DOE) was conducted comparing the effects of these changes on the mobility of the combined chassis and path-clearing-device system. Discrete events include both soft-soil and hard-surface. Events include half-rounds, potholes, grades, V-ditches, and cross country terrain.

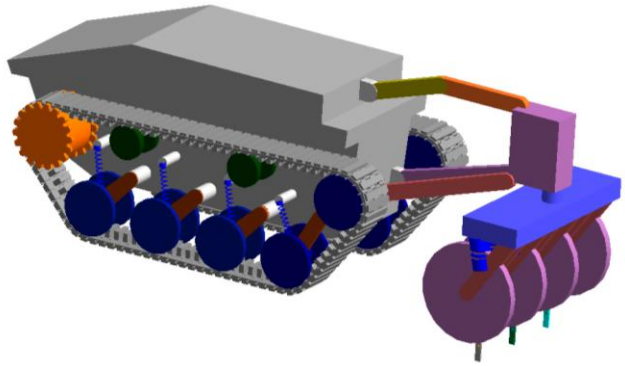

Figure 1: Notional vehicle with four road wheels per side, a band track, and a notional roller-rake path clearing implement attached.

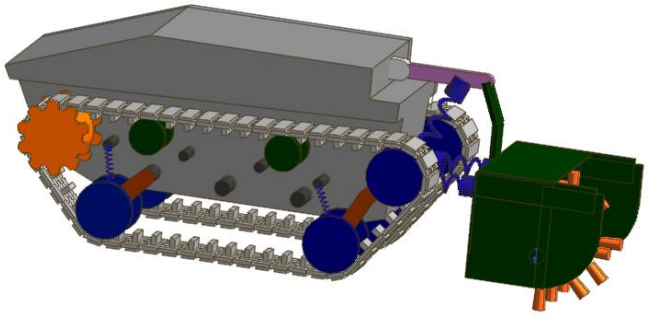

Figure 2: Notional vehicle with two road wheels per side, segmented track, and a notional flail path clearing implement attached.

To maintain the utility of the notional study for future specific designs, the extracted results were chosen so as to serve as a universal comparison between the changing variables on any generic design. The study compares load and acceleration responses in order to guide design recommendations. The methodology presented herein for applying soft soil terramechanics is unique in its ability to enhance the existing capabilities of Multi-Body Dynamics (MBD) software. The study presented was performed using the RecurDyn MBD software package. While the track-building toolkit within RecurDyn is helpful, the presented soft-soil modeling techniques are applicable to any code that allows for custom expressions and/or functions.

SOFT SOIL THEORY

The software used includes support for Bekker's pressure-sinkage soil model [1], a linear approximation of soil rebound during unloading (under the track only – no memory outside the track system exists), and the Janosi and Hanamoto shear stress-displacement relationship [1]. The vehicle-terrain models supported by the software were not modified for the purpose of this study.

Of major importance for this study are the methods for modeling shear failure of the soil at the path-clearing implement-to-terrain interaction. The Mohr-Coulomb failure criterion is one of the most widely used and is the basis of other models. The failure criterion is shown in Equation 1[2]:

$$\tau_{max} = c + \sigma \, tan\varphi \qquad (1)$$

where τ_{max} is the soils' maximum shearing strength, c is the cohesive strength of the soil, σ is the normal stress on the shearing surface, and φ is the soil's angle of internal friction [2].

Once this criterion is met in an idealized elastoplastic material, the surface provides no additional resistance as shear strain increases, as shown in Figure 3. This idealized elastoplastic assumption is not valid for all soil types, though it is suitable for modeling sand and clay [2].

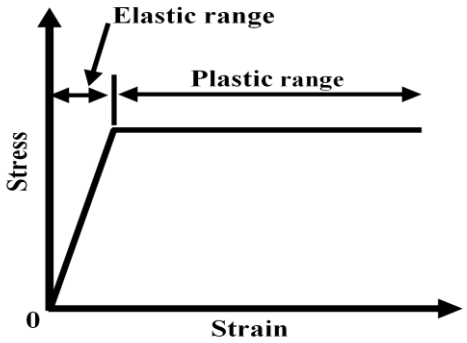

Figure 3: Stress-strain relationship of an idealized elastoplastic material

For this study, an application of the Mohr-Coulomb failure criterion is used to determine the passive soil resistance to a shearing surface, such as a rake. Figure 4 shows the Mohr circle for the active (expansive) and passive (compressive) failure strength of soil [3].

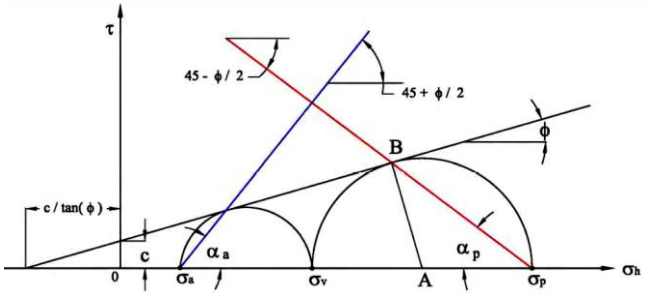

Figure 4: Mohr diagram for active (left circle) and passive (right circle) failure of soil.

The point of intersection between the passive failure circle and the horizontal axis of the Mohr diagram (Figure 4) determines the major principal stress, which is the lateral compressive stress required to set the soil at that point into passive failure [2]. According to the Mohr circle and as simplified according to previous research [4], passive failure occurs as shown in Equations 2-4:

$$\sigma_p = \gamma_s z \frac{1+sin\,(\varphi)}{1-sin\,(\varphi)} + 2c \frac{cos\,(\varphi)}{1-sin\,(\varphi)} \qquad (2)$$

$$\sigma_p = \gamma_s z * tan^2\left(45° + {}^{\varphi}/_{2}\right) + 2c * tan\left(45° + {}^{\varphi}/_{2}\right) \qquad (3)$$

$$\sigma_p = \gamma_s z * N_\varphi + 2c * \sqrt{N_\varphi} \qquad (4)$$

where $N_\varphi = tan^2(45° + \varphi/2)$, γ_s is specific weight of the terrain and z is the depth at the bottom of the failure region.

Nφ is known as the flow value and is related to the internal resistance of the terrain [2].

When there is external pressure (q) acting on the surface of the terrain, Equation 5 shows the passive failure stress[4].

$$\sigma_p = \gamma_s z N_\varphi + q N_\varphi + 2c\sqrt{N_\varphi} \quad (5)$$

Soft Soil Theory: Rake

When passive failure is caused by a physical device, such as a rake, with width (b) acting at a depth within the soil (h_b), Equation 6 models the passive failure resistive force of the terrain onto the device [5].

$$F_p = b * (0.5\gamma_s h_b^2 N_\varphi + q h_b N_\varphi + 2c h_b \sqrt{N_\varphi}) \quad (6)$$

The slip line field is composed of parallel lines sloped to the horizontal, the direction of the major principle stress, at *45°–φ/2*. Figure 5 shows the fully developed failure pattern as a blade moves horizontally through the terrain [2].

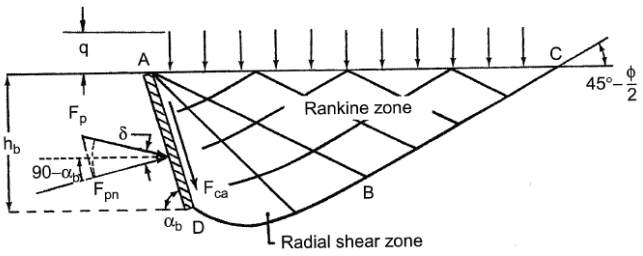

Figure 5: Fully developed failure patterns of soil in front of the vertical blade. F_{pn} is the passive failure force acting normal to the orientation of the shearing mechanism, F_{ca} is the frictional force between the soil and the shearing mechanism, and F_p is the combined resultant force. δ is the friction angle at the blade-soil interface, and α_b is the angle of the shearing mechanism from horizontal.

The Rankine Zone is the volume of resisting terrain under stress prior to plastic flow (failure) caused by expansion or compression of the soil (Area *ABC* in Figure 5) [2]. In a fully developed failure pattern in a terrain of high internal resistance, the Rankine Zone is very large compared to a terrain with low internal resistance.

Equation 6 above, using *Nφ* as the coefficient of passive failure can oversimplify the problem since it relies only on the soil properties while ignoring the friction on the rake blade-soil surface, assuming that the rake blade is perfectly vertical, and assuming the terrain is perfectly flat. As discussed in detail in the following section, Coulomb theory captures these additional parameters, and through the use of M&S, the resistive forces are recalculated at every time step based on the positions of the bodies in the simulation. Equation 7 models the passive earth coefficient K_p as calculated by Coulomb theory. Figure 6 shows the geometric Coulomb theory terms (ω, β), and δ is the friction angle at the blade-soil interface.

$$K_p = \frac{cos^2(\varphi+\omega)}{cos^2(\omega) * cos(\delta-\omega)\left[1-\sqrt{\frac{sin(\delta+\varphi)*sin(\varphi+\beta)}{cos(\delta-\omega)*cos(\beta-\omega)}}\right]^2} \quad (7)$$

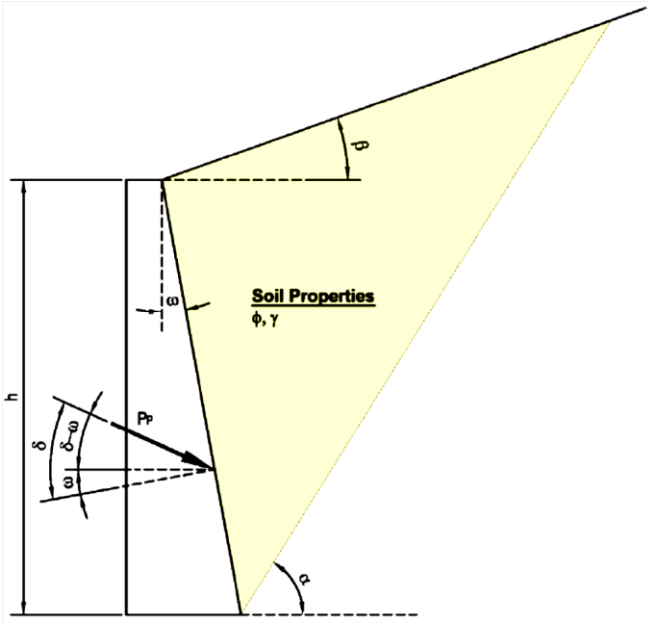

Figure 6: Classic lateral passive earth problem

K_p replaces N_φ in Equation 6 to calculate the resultant passive failure resistive force, as shown in Equation 8.

$$F_p = b * (0.5\gamma_s h_b^2 K_p + q h_b K_p + 2c h_b \sqrt{K_p}) \quad (8)$$

Soft Soil Theory: Flail Hammer Shear from Rapid, Non-Horizontal Input

Passive failure resistive force, as presented thus far, is a useful and accepted soil model for shear failure criterion [4]. However, what if soil failure patterns don't get fully developed? What if the direction of failure is not semi-infinite? Much of the science of terramechanics was explored at a time when numerical-based simulation methods were not yet a reality, and the models were developed to describe terrain forces on retaining walls. As a

result, many of the existing terramechanics formulae are from a static or quasi-static state, and damping and other rate-related terms aren't included. As a result, formulating a model of a flail is quite difficult.

The flail in this study causes soil failure by rapid impacts in an arc at a positive angle to the horizon. The soil failure arc means that the soil can't be considered semi-infinite and that the slip line fields aren't fully developed, as illustrated in Figure 7.

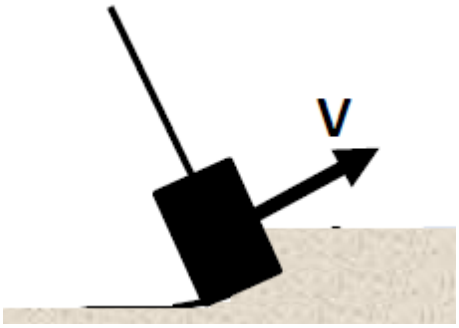

Figure 7: Flail hammer impact on soil.

The direction-of-failure issue is not easily solved. Models from literature on lateral earth pressure involving a moving blade assume that a vertical or slightly sloped blade is moving completely forward without any angular component. These models are analogous to a static retaining wall holding back earth. By the properties of friction, the frictional zone must develop to resist the motion at the failure surface (flail-terrain interface). Since the flail moves in an arc, the orientation of the elastically deformable region must change accordingly to resist the motion at the failure surface. A literature search for the appropriate model was conducted – and the Coulomb theory gave a powerful enough model that could be customized to fit this unique need. In a more traditional Coulomb passive earth problem, there would be a vertical or slightly sloped retaining wall holding an amount of soil which may be sloped with respect to the horizontal plane [3], as shown in Figure 6. Coulomb theory's passive earth parameters can be applied to the flail problem by substituting the retaining wall with the flail and re-orienting the terrain (and the slope of the terrain, β) with respect to the flail's shearing surface.

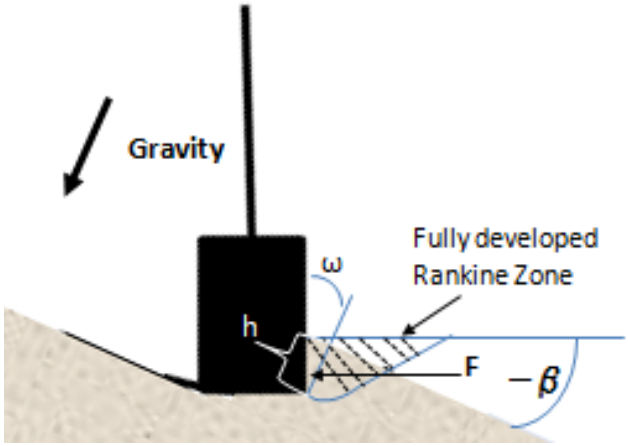

Figure 8: Reimagined Coulomb passive earth principle applied to the flail impact, re-oriented with respect to the vertical axis at an angle ω, showing that the Rankine Zone is not fully developed.

Since the terrain is not expected to move along the surface of the flail, flail-terrain friction forces can be assumed to be negligible. From Figure 8, $\omega = -\beta$. As a result, the passive lateral earth pressure coefficient (k_p) based on Coulomb's theory from Equation 7 simplifies according to Equation 9 [3], and this new coefficient K_p is applied to the resultant lateral resistive force according to Equation 8.

$$K_p = \frac{cos^2(\varphi+\omega)}{cos^3(\omega)*\left[1-\sqrt{\frac{sin(\varphi)*sin(\varphi-\omega)}{cos(-\omega)*cos(-2\omega)}}\right]^2} \quad (9)$$

Equations 6 and 8 modeled the lateral force taking into account an externally applied pressure on the surface. Usually, this pressure is the effect of the vehicle's weight on the surface of the soil. While the flail implement does not contact the surface of the terrain, the rollers on the roller-rake implement do contact the surface. However, since the rollers are narrow and do not apply a surcharge forward of the rake over the Rankine zone, this term will drop out in the resulting simulations.

Kinetic soil events could not be modeled for this study. Once the hammer hits the terrain, soil is rapidly accelerated to a significant speed and flung away. Energy is transferred from the hammer to the individual soil particles. However, there are no good models for these kinetic events. Simple assumptions could not be made - It would be difficult to guess the final speed of the soil particles, and one would imagine that cohesive and frictional terrains would behave differently. The force models presented are independent of

speed. While a faster object does require more power than a slower object to disrupt the terrain (Power = Force * Distance / Time), the passive failure resistance force is assumed to be the same regardless of speed. Some soil sampling studies have been performed at different speeds, however, the implications of a hammer traveling at very high velocities is unknown.

METHODOLOGY

The application of the soft-soil theory within MBD software and the Design of Experiments used to conduct the design and sensitivity study are detailed below. Major model parameters are given for the vehicle configurations and each of the path-clearing implements. Descriptions of the events are also presented. The methodology behind the sensitivity analysis is discussed at the end of this section.

Design of Experiments Setup

The experiment was set up as a partial factorial DOE over a set amount of events. There were three design variables and one sensitivity parameter (soft soil type); all altered between two distinct types or values. The prime mover either had two or four road wheels with a track that was made of segmented track linkages or band track. The path-clearance implement was either a flail or a roller-rake combination. Soil type was also varied between sand and clay, and is a sensitivity parameter. All possible combinations were run over a half-round bump event, pothole event, V-ditch event, and cross country terrain. The grade events were not run with all combinations. Table 1 summarizes the events tested. Table 2 summarizes the terrain information. Table 3 summarizes which designs were tested on which events.

Table 1: Design Factors

Factor	Abbreviation	Setting 1	Setting 2
Number of Road Wheels	RW#	2	4
Track Type	TTP	Segmented Links	Band
Implement	IMP	Flail	Roller-Rake
Soft Soil	SSL	Sand	Clay

Table 2: Mobility Events

Terrain	Abbrev.	Terrain Detail
Half-Round	HR	17.5 cm semi-circle / speed bump
Pothole	PH	17 cm deep by 60 cm long gap
V-Ditch	VD	1.4 m deep by 7.8 m long 'v'-shaped ditch
Grade	GRD	40%-70% grades; max grade traverseable reported
Cross Country	CCY	Cross country proving ground terrain

Table 3: DOE Setup

Factor	Events				
	HR	**PH**	**VD**	**GRD**	**CCY**
RW#	X	X	X	X	X
TTP	X	X	X	1*	X
IMP	X	X	X	X	X
SSL	X	X	X	X	2*

*1 – No effect of track type on simulation of grade or tilt table.
*2 – Clay only

Table 3 summarizes the partial factorial aspect of the DOE. Several simulations were conducted with only a single parameter changed to determine the overall effect of that parameter, and these events contribute to the sensitivity analysis as presented at the end of the Methodology section.

Common Vehicle Model Details

The overall goal for both the prime mover and implement designs was to be able to travel most places that a person could travel. The overall designs were simple and nonoptimized. However, the relative performance trends were apparent even with simple vehicle models.

From the experimental setup, there were three design variables (number of road wheels, track type, and implement) each with two settings. The chassis and several of the track geometries were constant for all simulations, as well as all mounting points for all suspension components and implement-mounting provisions. These constant parameters are presented in Table 4.

Table 4: Universal Vehicle Design Parameters

Constant Design Parameter	Value
Chassis Mass	450 kg
Overall Length (less implement)	2.1 m
Overall Width (less implement)	1 m
Wheelbase	1.13 m
Vehicle Track Width	0.746 m
Width of Individual Tracks	0.203 m
Chassis Roll Inertia	35.80 kg-m^2
Chassis Pitch Inertia	134.01 kg-m^2
Chassis Yaw Inertia	127.14 kg-m^2
Sprocket Carrier Radius	0.14 m
Road Wheel & Idler Radii	0.14 m

Design Factor Details: Number of Road Wheels

The design factor of two or four road wheels is the most straightforward configuration to model. The four road wheel configuration has four road wheels and four spring-dampers on each side, while the two road wheel configuration has two road wheels and two spring-dampers on each side. The two road wheel design is slightly lighter with the absence of the road wheels. The two road wheel design requires two stiffer springs in place of the four springs in the four road wheel design. The four road wheel configuration with segmented track is shown in Figure 9 to illustrate that the springs are oriented at a near tangent to the steady state position of the road arms' rotational arcs. The spring on the front road arm is located 23 cm from the road arm's mounting location (center of rotation), and all other springs are located 19.2 cm from their road arms' mounting location. The spring rates were adjusted for each of the eight design configurations to maintain the same ride height to better isolate the effects of changing the design parameters.

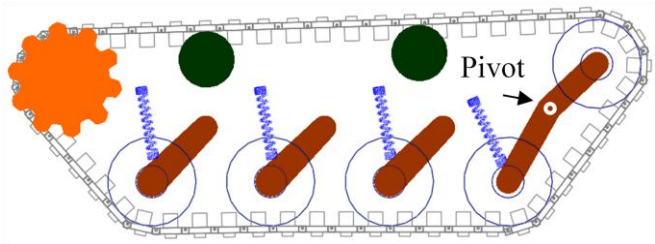

Figure 9: Track assembly of the four road wheel, segmented track configuration showing the orientation of the road arms and springs with the front link between the idler and first road wheel pivot point highlighted (used to maintain track tension).

Design Factor Details: Track Type

The handling of the track type design factor was more challenging – mainly because the MBD software utilized does not support a band track. As a result, a surrogate band track was modeled as a segmented track with many small links. This surrogate consists of 90 links as opposed to the "segmented track" factor which has 50 links. Another noticeable difference is the material properties between the band track and segmented track. The segmented track is primarily metal with rubber bushings and pads, while the notional band track was modeled primarily as rubber/neoprene with added carbon and KEVLAR®[1] fibers (reinforced rubber). The standard segmented track uses standard bushing-pin stiffness values as provided by the MBD program. However, this standard stiffness does not work for the band track. Since a real band track does not have discreet pins, the material properties dictate the longitudinal, lateral, and rotational stiffness properties. Published reinforced rubber material properties range according to the composition and degree of reinforcement of the band track. The chosen material properties for the band track were based upon tested reinforced rubber samples with 20% KEVLAR® engineered elastomer content [6]. The material's Young's Modulus (E) can be used to find the relationship between the resistive force of a material (F_m) to an amount of material strain ($\Delta L/L_0$) using the cross-sectional area of the track (A_0) [7], according to Equation 10. Equation 11 shows the Hooke's Law's equivalency between the stiffness (K) of multiple springs to a single representative spring (K_{eq}) [8]. Equations 12 and 13 show a simplified version of Hooke's Law where all constituent multiple springs have the same stiffness value. These relationships facilitate the necessary equivalency modeling between an engineered rubber's material properties to a segmented, linked track, as shown in Equations 14 and 15.

$$F_m = \frac{E*A_0*\Delta L}{L_0} \tag{10}$$

$$\frac{1}{K_{eq}} = \frac{1}{K_1} + \frac{1}{K_2} + \frac{1}{K_3} + \cdots + \frac{1}{K_n} \tag{11}$$

When $K_1 = K_2 = K_3 = \cdots = K_n = K$:

$$\frac{1}{K_{eq}} = \frac{1}{K_1} + \frac{1}{K_2} + \frac{1}{K_3} + \cdots + \frac{1}{K_n} = \frac{n}{K} \tag{12}$$

$$K = n * K_{eq} \tag{13}$$

Setting: $K_{eq} = \frac{E*A_0}{L_0}$ & $\Delta L = x$

$$F_m = \frac{E*A_0*\Delta L}{L_0} = K_{eq} * x \tag{14}$$

[1] KEVLAR is a registered trademark of of E. I. du Pont de Nemours and Company

$$K = n * \frac{E * A_0}{L_0} \quad (15)$$

Figure 10 shows the band track configuration with two road wheels (compare with Figure 9 above).

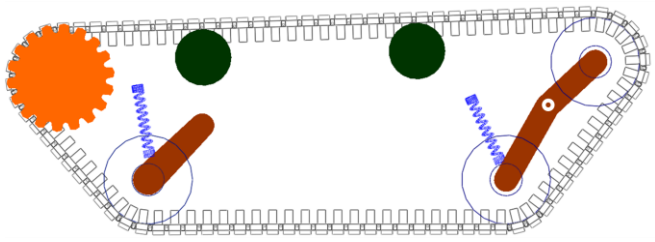

Figure 10: Track assembly of the two road wheel, band track configuration.

Design Factor Details: Path Clearing Implement

Two path clearing implements were designed and compared: a roller-rake and a flail. The flail consists of eighteen rotating conical hammers, a housing to surround the rotating elements, a central lift cylinder/hydraulic spring, pivot points to allow for raising and lowering of the housing which link back to the vehicle, and two springs which apply longitudinal force between the vehicle and the housing. The roller-rake consists of four roller-wheels, three rake-blades, springs to keep the rollers and blades in contact with the terrain, a rotational joint to facilitate turning/steering, rotational joints and linkages which connect the roller-rake to the vehicle while allowing for relative vertical motion.

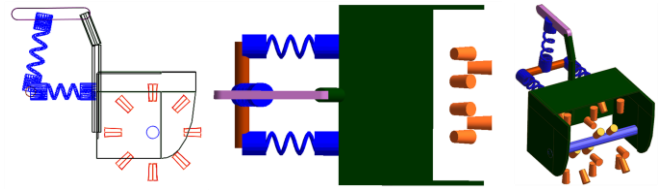

Figure 11: Side, top, and isometric views of the flail path-clearing implement

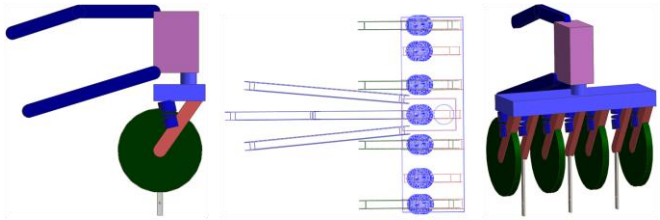

Figure 12: Side, top, and isometric views of the roller-rake path-clearing implement

The flail housing to vehicle mounting rotational joints allow for vertical motion of the flail. The vertical spring connecting the lower mounting provision to the upper mounting link also serves to raise and lower the housing as needed to avoid obstacles, such as a steep change in grade or vertical step. The flail's motor spins at a nominal speed of 40 rad/s. There are 9 sets of rotating hammer pairs. Each hammer pair is located at 180 degrees apart to counterbalance each other. The distance from the center of rotation to the tip of the hammer is 29.15 cm. The hammers clear a path 7 cm deep under nominal conditions, and can go as deep at 13.4 cm with multiple passes or at slow speed over weak terrain lowering the hydraulic lift cylinder. The flail's mass is 150 kg and the center of mass is located 65 cm forward of the vehicle's top-middle interface location. The motor is modeled as a constant-speed rotational motion. The average motor power and torque requirements are measured for each event and terrain.

The roller-rake's rotational joints on each end of the roller to vehicle attachment linkages allow for relative vertical motion between the vehicle and the implement. The joints also serve to maintain the upright position of the implement with torsional springs and geometric constraints. The center body that the attachment linkages attach to houses a rotational joint which allows the roller-rake to spin a full 360 degree roller yaw motion about the vertical axis to facilitate vehicle steering. The attachment linkages were designed to allow for enough clearance for this 360 degree yaw motion. The roller wheels are 25.4 cm radius. The rake blades are designed to penetrate the terrain up to 13 cm, though this will be less depending on the resistance the terrain is offering. The blades are mounted on trailing arms which have springs connecting them with the main implement housing to maintain the force needed to shear the terrain. As the shearing resistance increases, these springs will compress more which will lessen the depth of penetration and also lessen the shearing resistance from the terrain, based on Equation 6. The roller-rake's mass is 375 kg and the center of mass is located 91 cm forward of the vehicle's top-middle interface location.

Event Generation and Simulations

The events were generated according to the parameters in Table 2. The half-round, pothole, and cross country events were done at a speed of 2 m/s, as controlled at the vehicle's sprocket. The grades and V-ditches were performed at 1 m/s. Several of the events were performed over both sand and clay, while the others were performed over hard surface (see Table 3). The soil properties used to model the soils are shown in Table 5. For all simulations, the soil is homogenous and semi-infinite.

Table 5: Model Soil Properties of Sand and Clay**[4][9][10]**

Soil Property	**Sand**	**Clay**
Exponent Number (n) []	1.1	0.13
Terrain Stiffness (k_C) [kN/m^{1+n}]	0.99	12.7
Terrain Stiffness (k_φ) [kN/m^{2+n}]	1528.43	1555.95
Cohesion (c) [kN/m^2]	1.04	68.95
Shear Resistance Angle (φ) [rad]	0.70	0.35
Soil Flow Value (N_φ) []	4.60	2.04
Soil Specifc Gravity (γ) [N/m^3]	14.91	11.77
Blade-Terrain Interface Friction (δ) [rad]	14.91	11.77

While several of the values in Table 5 are used in the shear stress equations, others are used as parameters in the MBD program-supported pressure-sinkage capability.

To maintain the utility of the notional study for future specific designs, the extracted results are chosen to be a universal comparison between the changing variables on any generic design. The study compares load and acceleration responses in order to guide design recommendations. Load data was collected at each of the three vehicle-implement interface locations. Acceleration data was collected at the vehicle's center of gravity (CG). Peak magnitude data was collected for all events except for the cross country event, which was averaged instead. A steady state, at-rest, simulation was performed to collect the settled, overall center of gravity location of the vehicle-implement system.

Modeling Shear Stress

The soil theory section discussed the equations and models used to describe the soil shear resistance behavior. However, there are several unique challenges to apply these equations to an dynamically changing simulation.

All of the soil shear interface forces are calculated at each time step of the numerical simulation and act on the hammers or blades of the implement. A series of user-defined expressions were necessary to model the forces. Markers were created and placed on the implements as necessary to capture the necessary values to compute the current depth of the implement under the surface of the terrain. The markers have a standard X, Y, Z coordinate system which is used to ensure the resistive forces are always applied normal to the implements surface and to track the orientation of the hammer or blade. Once the marker's parent body is assigned to a body, the marker orients itself appropriately with that body. The X, Y, Z location of the marker is tracked by the global coordinate system, though as an option, the forces applied at the marker's location can be applied according to the marker's local coordinate system. Therefore, setting a force to be applied at the marker according to the marker's coordinate system, which reorients accordingly with the hammer or flail, the force will always be applied correctly.

The blade resistive force uses Equation 6 to compute the force magnitude since the blade is moving forward and the soil is semi-infinite relative to the blade's forward velocity. The depth of the blade is calculated by using a marker's global position and calculating the vertical distance at that longitudinal and lateral position. A logic statement checks the vertical relationship between the bottom of the blade and the terrain, so the force is only applied when the blade is beneath the terrain. Figure 13 shows the blade in the ground with the force applied.

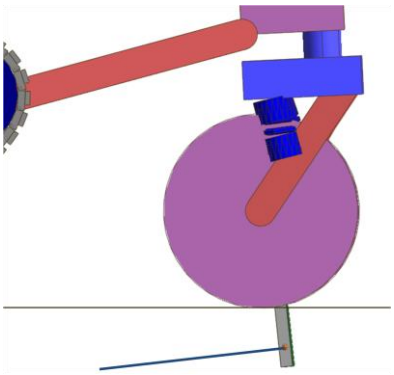

Figure 13: Blade penetrating the terrain while moving forward (to the right), showing the soil passive shear resistance vector, pointing to the left.

The hammer's resistive force is much more complicated than the blade's resistive force. The hammer uses a similar method for computing the depth of the hammer relative to the terrain and to ensure the force is applied in the right direction. However, there are a few extra details required for the hammer calculation. Since there are nine pairs of quickly rotating hammers, each hammer benefits from the terrain cleared from the other hammer in the pair. This relationship is shown in Figure 14. Figure 15 shows a zoomed in version of Figure 14. In Figure 14, V is the forward velocity of the flail implement and Δt is the known amount of time since the opposing hammer last hit.

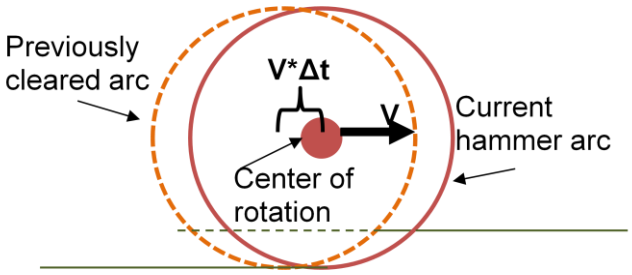

Figure 14: Successive hammer hits benefit from previous hits by reducing the amount of earth clearing required

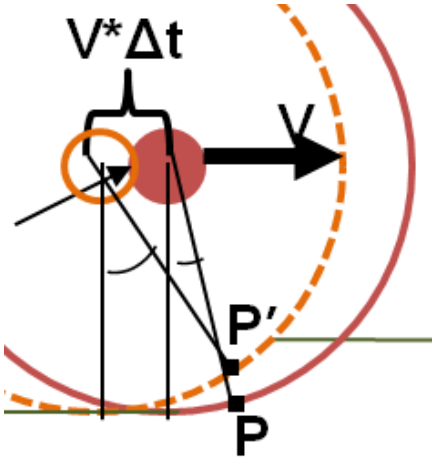

Figure 15: Close-up of Figure 14 showing the trigonometric relationship between the depth at P beneath the previously cleared terrain depth of P'

For a given point on the terrain to be cleared, *P*, there may be previously cleared terrain, which will reduce the amount of terrain to be cleared and therefore, reduce the resistance force. *P'* is the point at the same longitudinal and lateral position of *P* along the path of the previous hammer. The radius of the arc, longitudinal locations of the center of rotation, the point *P*, the angle on the arc at *P* (from a marker attached to the hammer), the previous center of rotation when the point at *P'* was cleared are all known values, it is straightforward to compute the relative height difference between *P* and *P'*. This relative height difference is the actual depth of terrain to be cleared, and replaces the h_b term in Equation 8 for calculating the total resistive force. A logic statement only applies this relative height difference when *P'* is below the surface of the terrain. If *P* is in uncleared terrain, the depth of *P* is calculated with the standard method. The flail's hammers have some amount of overlap, to ensure that the path is properly cleared. The flail's relative vertical position is also tracked between each hammer impact, so the depth between *P* and *P'* changes based on the flail's reaction to bumpy terrain.

Also, the hammers overlap to ensure the path gets cleared. This amount of overlap reduces the amount of terrain to be cleared. The flails are arranged so they are offset by plus and minus 45° from the neighboring hammers (see Figure 11). This leads to a stepped-clearance profile as shown in Figure 16. The change in time since the neighboring hammers impacted a given location can be calculated identically to what was done earlier, except the radial offset is 45° on one side and 135° on the other, instead of the 180° from the other hammer in the pair. For the purpose of the shear resistance calculation, the depth term for the cohesive resistance in Equation 8 is reduced by half of the difference of depth for each side. For example: if the depth would be 3 cm, but is 1 cm less on one side and 2 cm less on the other, the final depth for the cohesive term would be 1.5 cm. The internal friction term remains unchanged, except the cross-sectional area is reduced based on area of overlap. All of these logical checks and calculations are performed at each simulation step.

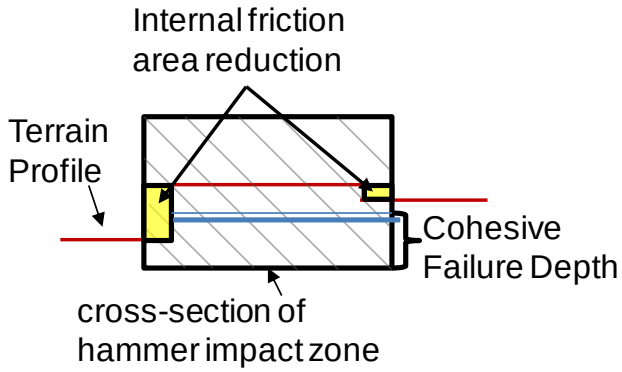

Figure 16: Uneven, stepped profile of hammer cross-sectional impact zone (hammer impact direction is into the page). The regions on the left and right were cleared by neighboring hammers. The box represents the cross-sectional area of the hammer.

Figure 17 shows the result of the user-defined hammer expressions. Three hammers are shown as penetrating the terrain. However, only two are being resisted because hammer A is in the zone of terrain that was previously cleared by its opposing hammer in the rotating pair. Since the half round itself is part of the terrain, the hammer within the half round (hammer C) is being resisted. The other resisted hammer (hammer B) is in a partially-cleared region. None of the other hammers are resisted by the terrain.

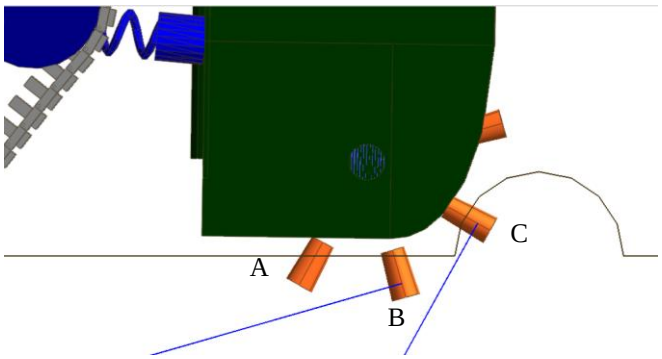

Figure 17: Hammer impacts with resistive force vectors shown

The resultant load profile of the flail motor is shown in Figure 18. This graph shows the motor torque required to maintain the 40 rad/s rotation speed while traveling at 2 m/s over flat clay and flailing at a depth of approximately 9 cm. For these conditions, an average torque of 130 N-m is needed, meaning that the power requirement to operate the flail under these conditions is 5200 W.

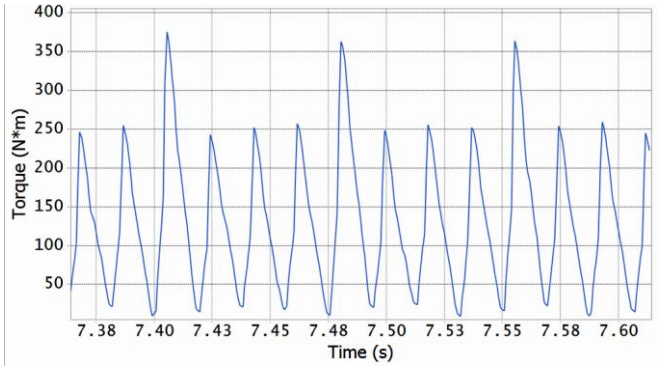

Figure 18: Flail's motor torque time history while traveling 2 m/s over flat clay.

The full effect of the study's application of passive soil failure is shown in Figure 19. This graph shows the motor torque required over a section of cross country terrain.

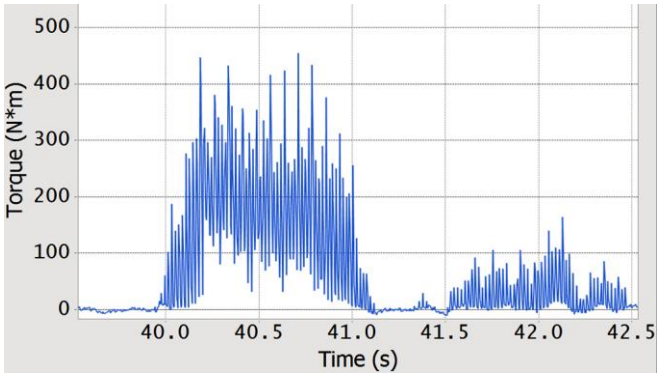

Figure 19: Flail's motor torque time history over a section of cross country terrain.

Sensitivity Analysis

Of potential value to future vehicle designs, sensitivity analyses were performed. A sensitivity analysis is vital whenever assumptions were made during the modeling process. This methodology provides for a strong scientific basis of the results. A sensitivity analysis gives a range of "good" values and will help future designers to choose notional design parameters. Without sensitivity values, the simulations performed are only good as good as the assumptions that were made, thus affecting the quality of the greater M&S findings. Another benefit is that it gives insight to the sensitivity of the manufacturing process of the items in questions. No two track-pin bushings are the same, nor are two band tracks. In general, sensitivity analyses/methodologies are vital to the M&S process in achieving real experimental benefit.

Three vehicle parameters were varied, independently as part of this sensitivity study. For each parameter, three simulations were performed, and all other aspects of the simulations remained constant. These analyses were simulated over the half-round event with clay terrain, and highlight the potential sensitivities in overall vehicle performance. The changed parameters for the sensitivity study are summarized in Table 6.

Table 6: Sensitivity Analysis Simulation Settings

Design Sensitivity	% Change Values from Default Design	Configuration Tested
Initial Track Bushing Tension / Preload	25%, 100%, 400%	4 Road Wheels, Segmented Track, No Implement
Band Track Stiffness (Youngs Modulus)	50%, 100%, 200%	4 Road Wheels, Band Track, No Implement
Track Link Backing Pad - Road Wheel Contact Stiffness	50%, 100%, 200%	4 Road Wheels, Segmented Track, No Implement

RESULTS

The complete set of simulation results are shown in the Appendix. This section highlights the performance effects of each of the design factors.

Results Details: Number of Road Wheels

The number of road wheels has a significant effect on the flotation/ground pressure of the tracks on the terrain. The biggest impact was on the pothole event which is representative of any short gap event. The two road wheel configuration fell into the pothole and had a large impact on the ascending edge of the pothole. The four road wheel configuration successfully floated over the top of the pothole without dropping into it, as shown in Figure 20. The loads and acceleration magnitude data were much more severe on the two road wheel configuration.

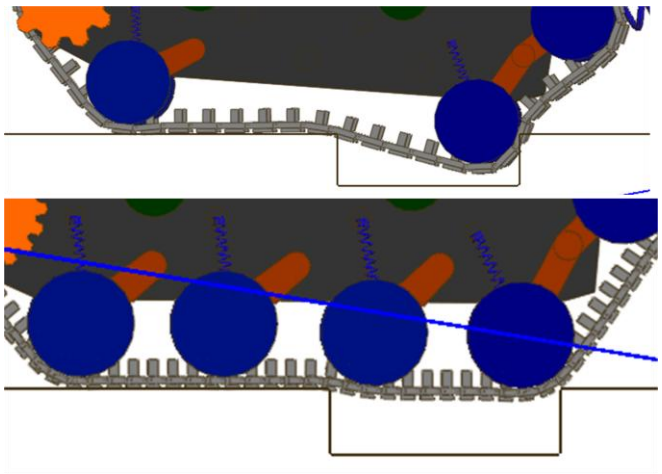

Figure 20: Comparison of four and two road wheel configurations over the pothole event.

Of particular note, the number of road wheels affected the mobility of the vehicle on grades. For cohesive soils such as clay, the maximum traction generated at the track-soil interface is equal to the cohesion of the soil multiplied by the track-soil contact patch [2]. Since four road wheels gives an effective higher contact patch than two road wheels, the four-wheeled configurations had the advantage on clay. For example, the configuration with the flail over clay with 4 road wheels successfully climbed a 55% grade (albeit slowly). However, the same configuration with 2 road wheels could not climb the 55% grade. The advantage was not universal, however. The two road wheel configuration performed better over sand. Since the two road wheel configuration had higher pressure under its wheels, it was able to dig in to generate higher traction while avoiding getting stuck, and it successfully traversed a 60% grade over sand. Of note, the configurations may have performed better on the grades if either the configuration was traveling at higher speed prior to the change of inclination or if the change in inclination was gradual. When moving at slow speeds over an abrupt change in grade, the vehicle's center road wheels lost contact with the ground as the front road wheel started its ascent. These leads to a smaller contact patch and results in a lower maximum tractive effort at the soil-track interface.

Results Details: Track Type

The track type had an impact on chassis vibration. The cross country analysis shows that the average magnitude of the acceleration loads were higher on the segmented track than on a band track. The average acceleration magnitude on the chassis over the cross country terrain was 0.42 g's on the segmented track and 0.36 g's on the band track, or 17% higher average g loads with the segmented track.

Results Details: Path Clearing Implement

The path clearing implement design factor had the biggest overall impact on vehicle dynamics performance. To better understand the effects of the path clearing implement, simulations were performed of the vehicle pushing each of the implements at 2 m/s, over both sand and clay, and over flat terrain without any other excitation. This allows for a direct view of how the implement weight, vehicle-implement interface loads, and soil loads on the implement balance out for the steady-state analysis. Since the moments about the center of gravity of the implement also must balance, there is a force multiplication on the loads at the brackets when there is an increase of loads at the implement-terrain surface. The directions of the forces on the implements are shown in Figure 21 and Figure 22, and the comparison of loads from the two terrain types are shown in Table 7 and Table 8.

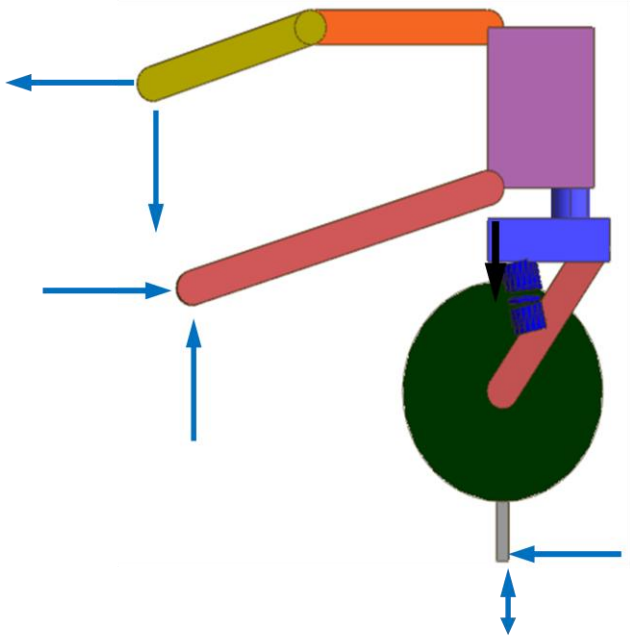

Figure 21: Two-dimensional view of the external forces acting on the roller-rake.

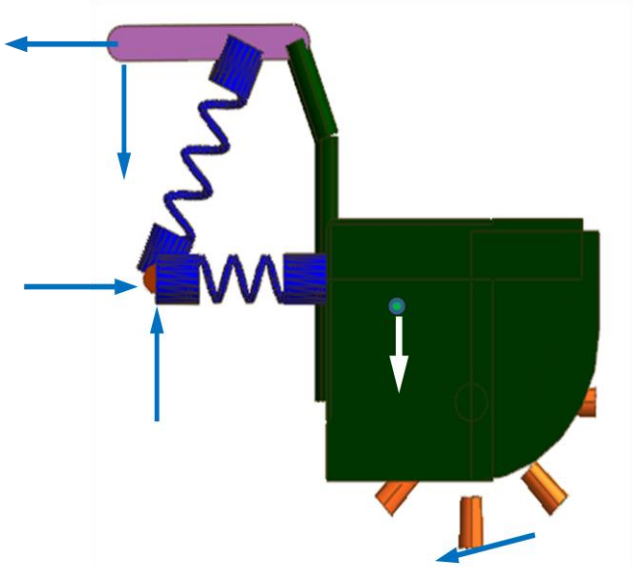

Figure 22: Two-dimensional view of the external forces acting on the flail.

Table 7: External Force summation on the roller-rake

Load Location	**Sum of Forces: +X Direction (lbs)**	
	Sand	Clay
Combined Lower Interface Brackets	984	3329
Upper Interface Bracket	-863	-2392
Rolling Resistance*	-51	-55
Blade Horizontal Force	-71	-899
Summation	**-1**	**-17**
Load Location	**Sum of Forces: +Y Direction (lbs)**	
	Sand	**Clay**
Combined Lower Interface Brackets	385	1078
Upper Interface Bracket	-33	-336
Wheel Normal Force	3348	2868
Blade Vertical Force	6	80
Weight	-3686	-3686
Summation	**20**	**4**

* modeled as a Coulomb friction element.

Table 8: External forces acting on the flail implement

Load Location	**Sum of Forces: +X Direction (lbs)**	
	Sand	**Clay**
Combined Lower Interface Brackets	1768	3017
Upper Interface Bracket	-1757	-2550
Hammer Impact Horizontal Force	-16	-469
Summation	**-5**	**-2**
Load Location	**Sum of Forces: +Y Direction (lbs)**	
	Sand	**Clay**
Combined Lower Interface Brackets	2153	2046
Upper Interface Bracket	-671	-414
Hammer Impact Vertical Force	-2	-164
Weight	-1472	-1472
Summation	**8**	-4

Of significant note, a large force at the terrain-implement interface has a large effect on the interface loads. Both the forces and moments about the implement's center of gravity (CG) must balance for a constant-velocity, steady-state simulation. Since the perpendicular distance is greater between the implement's CG and the ground than between the CG and the interface bracket's horizontal component, a

non-zero moment is generated from this force couple. This moment is counteracted by a pair of large counterforces between the different bracket locations. As a result, an increase in horizontal hammer load of about 450 N leads to increases of 650-850 N at each of the three interface locations. On the roller implement, an increase to the rake load has a significant impact on the vertical force couple at the brackets.

The implements were analyzed based on the peak dynamic loads at the vehicle-implement interface through the various events. The smaller the load at the interface for each event, the better. The flail performed significantly better over the pothole event, since the flail stays a few cm above the ground. The roller fell into the pothole and impacted the ascending edge of the pothole, as seen in Figure 23. The flail also had lower interface loads when negotiating the half round event, which was a surprise since the front of the flail impacts the half round, as shown in Figure 24. However, it should be noted that the angle of impact on the flail is low and the force was successfully absorbed by the flail's mounting springs. The roller, on the other hand, is more massive and pushes more force through the interface. The rake configuration imparted lower peak acceleration loads measured on the chassis, however. Similarly, the flail had lower interface loads but had larger chassis acceleration peaks than the rake over the V-Ditch event. The abrupt change in slope at the bottom of the "V" created a large impact load on the roller. The configuration with 2 road wheels with a rake and band track failed to ascend a clay V-Ditch and was stuck. This was the only configuration-terrain combination that failed to traverse the V-ditch. For the other configurations with the roller, the roller impacted the ascending slope of the "V", which greatly increased the loads at the interfaces, as shown in Figure 25.

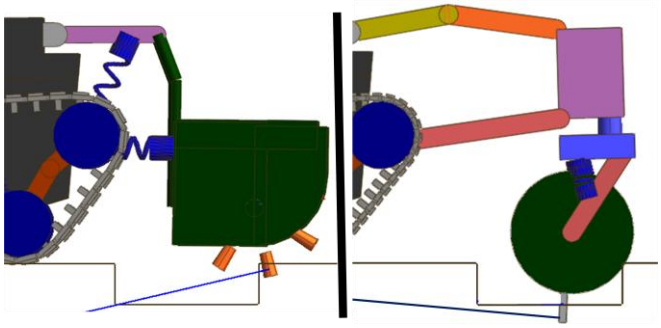

Figure 23: Comparison of the flail and roller-rake over the pothole event

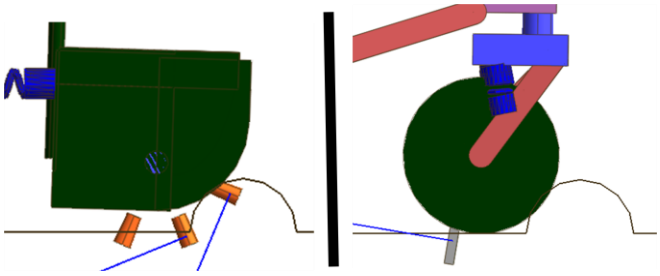

Figure 24: Comparison of the flail and roller-rake over the half round event

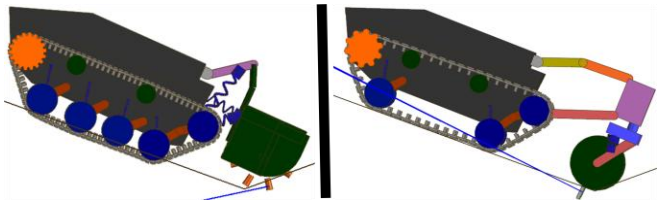

Figure 25: Comparison of the flail (over sand) and roller-rake (over clay) over the 'V'-ditch event

Sensitivity Analysis Results

The sensitivity analyses were performed at both steady-state, constant velocity (2 m/s) condition and over a half round event. The peak chassis acceleration magnitude was taken when the leading road wheel impacted the half round event. The steady-state acceleration magnitude was an average of 2 seconds of constant velocity and represents the vibration of the system imparted by the track system. The results from each set of sensitivity parameters are shown on Table 9, Table 10, and Table 11.

Table 9: Sensitivity Analysis on Band Track Material Properties

Young's Modulus [Mpa]	Radial "Bushing" Stiffness [kN/m]	Peak Chassis Acceleration Magnitude [g]	Steady State Chassis Acceleration Magnitudes [g]
47	5618	1.56	0.14
23.5	1433	1.36	0.21
94	11235	1.67	0.13

Table 10: Sensitivity Analysis on Segmented Track Initial Bushing Preload

Bushing Preload (N)	Peak Chassis Accelerations [g]	Steady State Chassis Acceleration Magnitudes [g]
500	1.34	0.28
125	1.31	0.29
2000	1.37	0.23

Table 11: Sensitivity Analysis on Road Wheel – Backing Rubber Pad Contact Interface of Segmented Track.

Track-Road Wheel Contact Stiffness (kN/m)	Peak Chassis Accelerations [g]	Steady State Chassis Acceleration Magnitudes [g]
3502	1.34	0.28
1751	1.28	0.24
7005	1.57	0.29

Changing these model parameters will have an effect on the chassis vibration / acceleration load results. Care must be taken to select the correct values or range of values. For the backing pad contact stiffness (Table 11), larger stiffness values at the contacts lead to larger vibrations. The bushing preload stiffness has a small effect on the peak chassis accelerations. However, there are other implications with increasing the initial bushing tension on the dynamic response of the vehicle that weren't modeled here, mainly that a higher bushing tension leads to greater ground pressure between road wheels [2].

DISCUSSION

The difficult challenge of taking static soil models and applying these models to an ever-changing, time based dynamics analysis was presented. Each hammer was modeled independently and saw a slightly different resistive force based on the simulated world. M&S best practices were presented. Steady-state force flow analyses and sensitivity analyses were performed to better analyze the system and the overall models' robustness. Results were generated and analyzed based on fairly rough designs, however, the performance patterns are apparent. The configuration with four road wheels per side, a band track, and operating the flail experienced the smallest interface loads over the pothole and half round events and seem to offer the best performance. The flail offered the greatest universal benefit in interface loads across all events. The two road wheel configuration performed better on sand over grades, however, and several events had less chassis acceleration magnitude loads with the rake attached.

Of particular note is where the current models are lacking. The damping or speed-of-failure behavior of the soil weren't effectively modeled. Also, the kinetic energy transfer from the hammer to the soil particles as they were flung away was not modeled. Suitable models simply do not exist and there are too many unknowns to develop simple assumptions. These soil behaviors needs should be explored in detail, and both future and current M&S software will benefit from the analysis of soil behavior.

REFERENCES

[1] FunctionBay, Inc., "RecurDyn/ Solver Theoretical Manual," FunctionBay, Inc., Republic of Korea, 2012.

[2] J. Y. Wong, Terramechanics and Off-Road Vehicle Engineering - 2nd ed., Oxford, UK: Elsevier Ltd, 2010.

[3] California Department of Transportation, "Trenching and Shoring Manual," California Department of Transportation, California, 2011.

[4] J. Y. Wong, Theory of Ground Vehicles - 4th ed., Hoboken, New Jersey: John Wiley & Sons, 2008.

[5] K. Terzaghi, Theoretical Soil Mechanics, New York, Wiley, 1943.

[6] E. I. duPont de Nemours and Company, "KEVLAR engineered elastomer with NeopreneGRT," [Online]. Available: http://www2.dupont.com/Kevlar/en_US/assets/downloads/d.%20%201F735%20Neoprene%20GRT%20Matrix.pdf. [Accessed 8 August 2012].

[7] F. P. Beer, J. E. Russel Johnston and J. T. DeWolf, Mechanics of Materials, 3rd ed., New York: McGraw-Hill, 2002.

[8] D. J. Inman, Engineering Vibrations, 2nd ed, Upper Saddle River, NJ: Prentice-Hall, Inc., 2001.

[9] Environmental Science Division, Argonne National Laboratory, "Soil Density," [Online]. Available: http://web.ead.anl.gov/resrad/datacoll/soildens.htm. [Accessed 2013].

[10] S. F. Bartlett, "Earth Pressure Theory," 11 March 2010. [Online]. Available: http://www.civil.utah.edu/~bartlett/CVEEN6920/Earth%20Pressure%20Theory.pdf.

APPENDIX

Table 12: Pothole Results

CONFIGURATION								Force Magnitude Results by Bracket Location [N]			Acceleration Magnitude at Chassis CG [g]
Clay	Sand	Band	Sgmt	2 RW	4 RW	Flail	Roller	Lwr_Rgt	Lwr_Lft	Uppr	G_load
X		X		X		X		3630	3641	5343	2.38
X		X			X	X		3036	3114	4340	1.32
X			X	X		X		4699	4414	5898	2.40
X			X		X	X		4339	4277	5836	2.09
	X	X		X		X		2413	2222	3169	2.12
	X	X			X	X		2343	2159	2885	1.55
	X		X	X		X		2960	2897	3711	1.46
	X		X		X	X		2383	2814	3212	2.06
X		X		X			X	16164	16215	18519	2.42
X		X			X		X	15922	15892	19328	2.09
X			X	X			X	15954	16560	17985	2.35
X			X		X		X	16098	16216	20277	2.73
	X	X		X			X	5933	5921	7865	2.91
	X	X			X		X	5439	5604	6913	2.78
	X		X	X			X	6655	6830	7351	2.71
	X		X		X		X	4340	4538	4549	2.07
AVERAGE BAND TRACK								6860	6846	8545	2.20
AVERAGE SEGMENTED TRACK								7179	7318	8602	2.24
AVERAGE TWO ROAD WHEEL								7301	7338	8730	2.34
AVERAGE FOUR ROAD WHEEL								6738	6827	8418	2.09
AVERAGE FLAIL								3225	3192	4299	1.92
AVERAGE RAKE								10813	10972	12848	2.51

Table 13: Half Round Results

CONFIGURATION								Force Magnitude Results by Bracket Location [N]			Acceleration Magnitude at Chassis CG [g]
Clay	Sand	Band	Sgmt	2 RW	4 RW	Flail	Roller	Lwr_Rgt	Lwr_Lft	Uppr	G_load
X		X		X		X		4731	5250	5478	2.39
X		X			X	X		4652	4246	6357	2.80
X			X	X		X		4524	4488	6253	3.28
X			X		X	X		4417	4846	6509	3.51
	X	X		X		X		3633	3536	5170	1.31
	X	X			X	X		3010	3035	3985	1.08
	X		X	X		X		3357	3190	4519	1.29
	X		X		X	X		3177	2692	4658	1.05
X		X		X			X	8026	8035	9558	2.09
X		X			X		X	8372	8343	10559	1.36
X			X	X			X	10605	10694	14265	2.24
X			X		X		X	8967	9080	12309	1.71
	X	X		X			X	6956	6758	7247	1.23
	X	X			X		X	6680	6436	6779	1.17
	X		X	X			X	5447	4977	6047	1.48
	X		X		X		X	7173	6928	7129	1.06
AVERAGE BAND TRACK								5758	5705	6892	1.68
AVERAGE SEGMENTED TRACK								5958	5862	7711	1.95
AVERAGE TWO ROAD WHEEL								5910	5866	7317	1.91
AVERAGE FOUR ROAD WHEEL								5806	5701	7286	1.72
AVERAGE FLAIL								3938	3910	5366	2.09
AVERAGE RAKE								7778	7656	9237	1.54

Table 14: Performance on Grades

Configuration	Steepest Grade Traversed	Notes
2 road wheels, Flail, Over Sand	60% grade	5400 W of sprocket power, not including flail operation
4 road wheels, Flail, Over Sand	55% grade	
2 road wheels, Flail, Over Clay	45% grade	
4 road wheels, Flail, Over Clay	55% grade	
2 road wheels, Rake, Over Sand	60% grade	7540 W of sprocket power needed
4 road wheels, Rake, Over Sand	60% grade	
2 road wheels, Rake, Over Clay	35% grade	
4 road wheels, Rake, Over Clay	40% grade	

Table 15: Average Load and Acceleration Results over Cross Country

Configuration						Average Force Magnitude Results by Bracket Location [N]			Average Acceleration Magnitude at Chassis CG [g]
Band	Sgmntd	2 RW	4 RW	Flail	Roller	Lwr_Rgt	Lwr_Lft	Uppr	G_load
X		X		X		1769	1680	2411	0.39
X			X	X		1485	1424	1963	0.30
	X	X		X		1469	1416	1919	0.43
	X		X	X		1642	1649	2302	0.37
X		X			X	1947	1776	2393	0.45
X			X		X	1722	1586	2054	0.30
	X	X			X	2089	1683	2465	0.50
	X		X		X	2014	1656	2378	0.37
AVERAGE BAND TRACK						1731	1617	2205	0.36
AVERAGE SEGMENTED TRACK						1804	1601	2266	0.42
AVERAGE TWO ROAD WHEEL						1819	1639	2297	0.44
AVERAGE FOUR ROAD WHEEL						1716	1579	2174	0.34
AVERAGE FLAIL						1591	1542	2149	0.37
AVERAGE RAKE						1943	1675	2323	0.41

Table 16:V-Ditch Results

CONFIGURATION								Force Magnitude Results by Bracket Location [N]			Acceleration Magnitude at Chassis CG [g]	Passed?
Clay	Sand	Band	sgmntd	2 RW	4 RW	Flail	Roller	Lwr_Rgt	Lwr_Lft	Uppr	G_load	Yes
X		X		X		X		2687	2546	4036	3.98	Yes
X		X			X	X		3916	2480	6331	1.95	Yes
X			X	X		X		1862	3339	5349	0.98	Yes
X			X		X	X		3872	2339	5421	1.09	Yes
	X	X		X		X		1913	1749	3484	0.81	Yes
	X	X			X	X		2498	2228	5146	1.04	Yes
	X		X	X		X		2023	1960	3685	0.66	Yes
	X		X		X	X		1886	1918	3819	0.64	Yes
X		X		X			X	5699	5739	7070	2.21	No
X		X			X		X	5323	5246	6930	1.22	Yes
X			X	X			X	5042	4988	6849	1.46	Yes
X			X		X		X	4973	4948	6840	0.71	Yes
	X	X		X			X	4444	4412	5184	0.96	Yes
	X	X			X		X	3516	3479	4659	0.81	Yes
	X		X	X			X	3345	3586	5683	0.74	Yes
	X		X		X		X	3945	3917	5156	0.59	Yes
AVERAGE BAND TRACK								3750	3485	5355	1.62	
AVERAGE SEGMENTED TRACK								3369	3374	5350	0.86	
AVERAGE TWO ROAD WHEEL								3377	3540	5168	1.47	
AVERAGE FOUR ROAD WHEEL								3741	3319	5538	1.01	
AVERAGE FLAIL								2582	2320	4659	1.39	
AVERAGE RAKE								4536	4539	6046	1.09	